Author/s:
Chua, MJ;Tng, J;Hesping, E;Fisher, GM;Goodman, CD;Skinner-Adams, T;Do, D;Lucke, AJ;Reid, RC;Fairlie, DP;Andrews, KT

Title:
Histone deacetylase inhibitor AR-42 and achiral analogues kill malaria parasites in vitro and in mice

Date:
2021-12-01

Citation:
Chua, M. J., Tng, J., Hesping, E., Fisher, G. M., Goodman, C. D., Skinner-Adams, T., Do, D., Lucke, A. J., Reid, R. C., Fairlie, D. P. & Andrews, K. T. (2021). Histone deacetylase inhibitor AR-42 and achiral analogues kill malaria parasites in vitro and in mice. International Journal for Parasitology Drugs and Drug Resistance, 17, pp.118-127. https://doi.org/10.1016/j.ijpddr.2021.08.006.

Persistent Link:
https://hdl.handle.net/11343/290080

International Journal for Parasitology: Drugs and Drug Resistance 17 (2021) 118–127

Contents lists available at ScienceDirect

International Journal for Parasitology: Drugs and Drug Resistance

journal homepage: www.elsevier.com/locate/ijpddr

Histone deacetylase inhibitor AR-42 and achiral analogues kill malaria parasites *in vitro* and in mice

Ming Jang Chua [a,1], Jiahui Tng [b,1], Eva Hesping [a], Gillian M. Fisher [a], Christopher D. Goodman [c], Tina Skinner-Adams [a], Darren Do [b], Andrew J. Lucke [b], Robert C. Reid [b], David P. Fairlie [b,**], Katherine T. Andrews [a,*]

[a] Griffith Institute for Drug Discovery, Griffith University, Queensland, 4111, Australia
[b] Institute for Molecular Bioscience, The University of Queensland, Queensland, 4072, Australia
[c] School of BioSciences, The University of Melbourne, Victoria, 3010, Australia

ARTICLE INFO

Keywords:
P. falciparum
HDAC inhibitor
Malaria
AR-42

ABSTRACT

Malaria is caused by infection with *Plasmodium* parasites and results in significant health and economic impacts. Malaria eradication is hampered by parasite resistance to current drugs and the lack of a widely effective vaccine. Compounds that target epigenetic regulatory proteins, such as histone deacetylases (HDACs), may lead to new therapeutic agents with a different mechanism of action, thereby avoiding resistance mechanisms to current antimalarial drugs. The anticancer HDAC inhibitor AR-42, as its racemate (*rac*-AR-42), and 36 analogues were investigated for *in vitro* activity against *P. falciparum*. *Rac*-AR-42 and selected compounds were assessed for cytotoxicity against human cells, histone hyperacetylation, human HDAC1 inhibition and oral activity in a murine malaria model. *Rac*-AR-42 was tested for *ex vivo* asexual and *in vitro* exoerythrocytic stage activity against *P. berghei* murine malaria parasites. *Rac*-AR-42 and 13 achiral analogues were potent inhibitors of asexual intraerythrocytic stage *P. falciparum* 3D7 growth *in vitro* (IC_{50} 5–50 nM), with four of these compounds having >50-fold selectivity for *P. falciparum* versus human cells (selectivity index 56–118). *Rac*-AR-42 induced *in situ* hyperacetylation of *P. falciparum* histone H4, consistent with *Pf*HDAC(s) inhibition. Furthermore, *rac*-AR-42 potently inhibited *P. berghei* infected erythrocyte growth *ex vivo* (IC_{50} 40 nM) and *P. berghei* exoerythrocytic forms in hepatocytes (IC_{50} 1 nM). Oral administration of *rac*-AR-42 and two achiral analogues inhibited *P. berghei* growth in mice, with *rac*-AR-42 (50 mg/kg/day single dose for four days) curing all infections. These findings demonstrate curative properties for HDAC inhibitors in the oral treatment of experimental mouse malaria.

1. Introduction

Malaria remains a leading cause of parasite-induced morbidity and mortality worldwide. In 2019, an estimated 229 million malaria cases and 409,000 malaria related deaths were reported, with most deaths occurring in Sub-Saharan Africa due to infection with *Plasmodium falciparum* (World Health Organization, 2020). Although there are effective drugs available for malaria prevention and treatment, including the gold standard artemisinin combination therapies (ACTs), parasite resistance to all current therapies and the lack of a widely effective vaccine are driving new antimalarial drug discovery efforts (Burrows et al., 2017; Phillips et al., 2017).

Growing evidence of the significance of epigenetics in *P. falciparum* (Andrews et al., 2012a; Bechtsi and Waters, 2017; Bozdech et al., 2003; Chaal et al., 2010; Coleman et al., 2014; Duraisingh et al., 2005; Freitas-Junior et al., 2005; Lopez-Rubio et al., 2007) suggests that epigenetic regulatory proteins may be promising drug targets for malaria (Andrews et al., 2012b; Coetzee et al., 2020; Malmquist et al., 2012). Furthermore, a potentially useful strategy in malaria drug discovery is to "piggy-back" onto drug development programs for other diseases, either by exploiting a common target or by using or improving upon validated inhibitors (Andrews et al., 2014). Anticancer epigenetic inhibitors are being investigated against malaria parasites, with histone deacetylase (HDAC) inhibitors being the most extensively investigated to date (Andrews

* Corresponding author.
** Corresponding author.
E-mail addresses: d.fairlie@uq.edu.au (D.P. Fairlie), k.andrews@griffith.edu.au (K.T. Andrews).
[1] These authors contributed equally.

https://doi.org/10.1016/j.ijpddr.2021.08.006
Received 1 June 2021; Received in revised form 17 August 2021; Accepted 20 August 2021
Available online 23 August 2021

et al., 2009, 2012b; Chua et al., 2017; Engel et al., 2015; Malmquist et al., 2012; Sumanadasa et al., 2012). Vorinostat (Zolinza®), romidepsin (Istodax®), belinostat (Beleodaq®) and panobinostat (Farydak®) are broad spectrum HDAC inhibitors approved for treating human cancers and have *in vitro* antiplasmodial activity (Chua et al., 2017; Engel et al., 2015). Although these compounds have potent *in vitro* antiplasmodial activity (IC_{50} 7–370 nM; Supplementary data, Table S1) (Chua et al., 2017; Engel et al., 2015), they lack high selectivity for *Plasmodium* over human cells (selectivity index (SI) < 1 (romidepsin); 7–21 (belinostat); Supplementary data, Table S1 (Chua et al., 2017; Engel et al., 2015)). *In vivo* assessments of HDAC inhibitors in murine malaria models have demonstrated limited effectiveness and not cured infection when administered orally (Agbor-Enoh et al., 2009; Andrews et al., 2000; Chua et al., 2017; Darkin-Rattray et al., 1996; Dow et al., 2008; Sumanadasa et al., 2012).

We hypothesize that poor *in vivo* efficacy of HDAC inhibitors investigated to date is due, in part, to suboptimal pharmacokinetic profiles (e.g. vorinostat, panobinostat; Supplementary data, Table S2) (Chua et al., 2017). Like vorinostat and panobinostat, the phenylbutyrate analogue AR-42 (Lu et al., 2004, 2005) targets multiple class I/II human HDACs but has superior pharmacokinetic properties in mice and humans (Supplementary data, Table S2). AR-42 is reportedly safe and well tolerated (Sborov et al., 2017; Valencia et al., 2016) and is undergoing clinical trials for different cancers (Chen et al., 2017; ClinicalTrials.gov, 2017a, b; Sborov et al., 2017). It has previously demonstrated *in vitro* activity against asexual and gametocyte (stage I-II) *P. falciparum* parasites (>50% inhibition at 1 μM) (Vanheer et al., 2020). AR-42 is (*S*)-*N*-hydroxy-4-(3-methyl-2-phenyl-butanamido)-benzamide), with a single chiral centre prone to racemization and to chemical reactivity due to its relatively acidic α-CH. It is 5-fold more potent as an inhibitor of HDACs (IC_{50} 16 nM) than its *R*-enantiomer (IC_{50} 84 nM). To avoid racemization and minimise metabolism, a series of achiral analogues of AR-42 were developed (Tng et al., 2020). They proved to be up to 35-fold more potent inhibitors of hHDAC1 and other class I HDACs than *rac*-AR-42 (compound **1**, Table 1) (Tng et al., 2020). Here, we investigated *in vitro* antiplasmodial activity of **1** and 36 synthetic analogues (including 31 achiral compounds; Table 1) and assessed *in vivo* activity of **1** and four analogues in *P. berghei* infected mice.

2. Materials and methods

2.1. Synthesis of achiral analogues of AR-42

Most compounds were synthesized as described (Tng et al., 2020). A small modification to the published protocol was used to synthesize new compounds **34**–**37** (Supplementary data, Scheme S1).

2.2. In vitro P. falciparum growth inhibition assays

In vitro antiplasmodial activity was tested against *P. falciparum* over 48 h in a [^{3}H]-hypoxanthine uptake isotopic microtest, as described (Chua et al., 2017). Assays were performed starting with asynchronous *P. falciparum* parasites (1% parasitemia; 1% haematocrit). Uninfected erythrocyte background controls were included in all assays. Negative controls containing *P. falciparum* infected erythrocytes treated with DMSO vehicle were included on each plate (0.5%; Sigma-Aldrich, USA). Percentage growth inhibition was calculated relative to negative DMSO vehicle controls after background subtraction and 50% growth inhibition concentrations (IC_{50}) were calculated using linear interpolation of dose response curves (Huber and Koella, 1993). At least three independent assays were conducted, each in triplicate. Pearson correlation analyses, to compare IC_{50} with cLog *P* values, were performed in GraphPad Prism 6.

2.3. Cell cytotoxicity assays

Cytotoxicity was assessed on human neonatal foreskin fibroblasts (NFFs), as described (Trenholme et al., 2014). In each case, three independent experiments were performed, each in triplicate. Percentage growth inhibition was calculated using DMSO vehicle treated cells as 100% growth and IC_{50} values calculated using log linear interpolation (Huber and Koella, 1993).

2.4. In vivo efficacy in a murine model of malaria

In vivo efficacy was evaluated in female BALB/c mice infected via intraperitoneal injection with *P. berghei* QIMR or ANKA (Saul et al., 1997) infected erythrocytes from a passage mouse (10^5 infected erythrocytes/100 μL). Mice were treated via oral gavage with 100 μL/dose of vehicle control (50% DMSO: 50% PBS) or test compounds for four consecutive days, beginning 2 h post infection (p.i.). Chloroquine (10 mg/kg; single daily doses) or vorinostat (25 mg/kg; twice daily doses) were used as positive controls. Mice were scored for symptoms and, from day 4 p.i., via microscopic analysis of DiffQuik® (POCD Healthcare, Australia) stained thin blood smears prepared via tail snip every 1–3 days. For each timepoint, parasites in at least 1000 erythrocytes were counted and parasitemia determined as mean number of parasites/100 erythrocytes. Mice were euthanized when parasitemia reached ~15–25%, or when weight loss compared to the day of infection exceeded ~15%, according to an approved Griffith University Animal Ethics Committee project (ESK/02/17/AEC).

2.5. Protein hyperacetylation assays

Protein hyperacetylation assays were conducted by incubating trophozoite stage *P. falciparum* 3D7 parasites (3–5% parasitemia; 5% haematocrit) for 3 h with 5x IC_{50} AR-42, vorinostat (HDAC inhibitor control) or chloroquine (negative control). Parasite infected erythrocyte pellets were lysed with 0.15% saponin, washed with PBS, resuspended in 1x SDS loading dye and heated at 94 °C for 3 min. Protein samples were analysed by SDS-PAGE and Western blot. REVERT™ Total Protein Stain (Li-Cor Biosciences, USA) was used to detect total protein. Anti-(tetra)acetyl histone H4 antibody (1:2,000 dilution; Millipore; 06–866) was used as a primary antibody and IRDye® 680RD goat anti-rabbit (1:10,000 dilution; Li-Cor Biosciences, USA) as a secondary antibody. Membranes were imaged using a Versadoc™ system (Li-Cor Biosciences, USA) and densitometry analyses conducted using Image Studio Lite v5.2 software.

3. Results and discussion

3.1. Structure-activity relationships for antiplasmodial activity

AR-42 has a typical HDAC inhibitor structure, comprising a *zinc-binding group* (hydroxamate) attached to a *linker group* (*para*-aminobenzoic acid) joined to a *capping group* (*3S*-methyl-2-phenylbutyric acid) via an amide bond. To remove the racemizable chiral centre, a series of achiral analogues were synthesized (Supplementary data) with a geminal dialkyl substituent or a symmetrical ring linked via a quaternary carbon atom instead of the isopropyl group of AR-42 (Tng et al., 2020).

In vitro antiplasmodial activity of *rac*-AR-42 (**1**) and 36 analogues was assessed against asexual intraerythrocytic stages of the drug-sensitive *P. falciparum* 3D7 line (*Pf*3D7; Table 1). Compound **1** had IC_{50} 22 nM, consistent with a previous report (100% inhibition at 120 nM) (Vanheer et al., 2020), and well below C_{max} of oral **1** in mice or humans (C_{max} 14.7 μM (single 50 mg/kg oral dose) or 0.38 μM (single 20 mg oral dose), respectively; Supplementary data, Table S2). The *N*-methyl analogue **2** (IC_{50} 1.2 μM; Table 1) was 60-fold less potent than **1** ($p < 0.0001$), consistent with the amide NH creating a H-bond

Table 1
Rac-AR-42 and 36 achiral analogues inhibit the proliferation of asexual blood-stage *P. falciparum* 3D7 malaria parasites and recombinant human HDAC1.

Entry	Structure	IC_{50} (nM)		Entry	Structure	IC_{50} (nM)	
		*Pf*3D7	hHDAC1			*Pf*3D7	hHDAC1
1 ***(rac*-AR-42)**	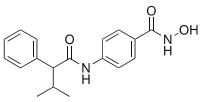	22 ± 3	25 ± 6	**20** (JT83)	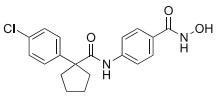	5 ± 3	14 ± 11
2	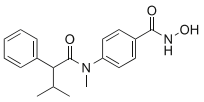	1229 ± 102	439 ± 47	**21**	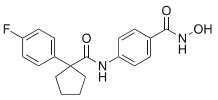	12 ± 3	41 ± 7
3	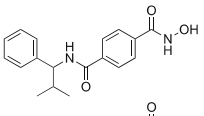	3559 ± 1426	2116 ± 749	**22**	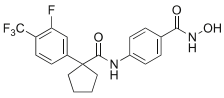	233 ± 22	222 ± 142
4	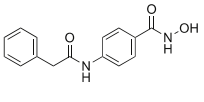	314 ±37	75 ± 13	**23**	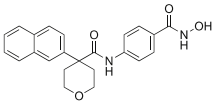	32 ± 11	0.7 ± 0.3
5	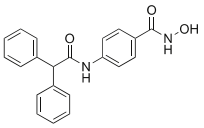	140 ± 64	250 ± 137	**24**	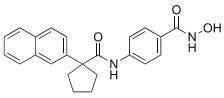	591 ± 223	11 ± 5
6	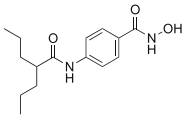	719 ± 583	738 ± 145	**25**	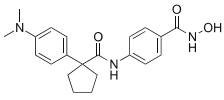	202 ± 5	4 ± 1
7	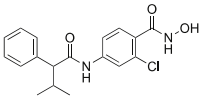	1092± 1069	8680 ± 4800	**26**	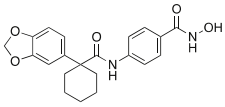	384 ± 194	42 ± 31
8	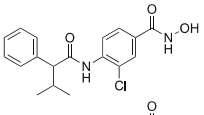	>10,000	1065 ± 753	**27**	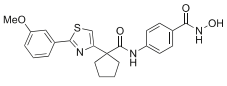	441 ± 46	15 ± 8
9	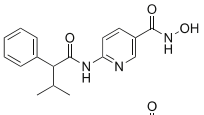	230 ± 37	22 ± 16	**28**	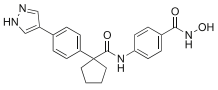	26 ± 18	2 ± 0.6
10	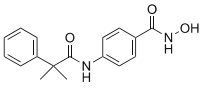	212 ± 16	218 ± 42	**29**	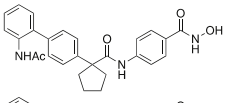	409 ± 76	0.9 ± 0.6
11	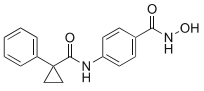	769 ± 193	430 ± 92	**30**	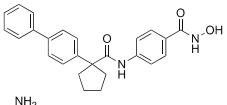	730 ± 155	16 ± 5
12	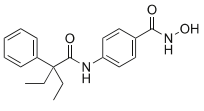	74 ± 8	93 ± 24	**31**	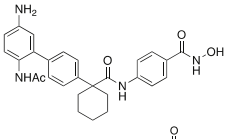	683 ± 445	10 ± 6
13	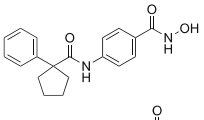	35 ± 11	28 ± 6	**32**	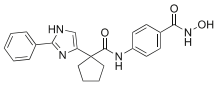	19 ± 3	4 ± 1
14	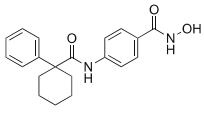	14 ± 3	15 ± 5	**33**	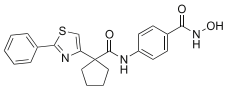	232 ± 28	12 ± 5
15	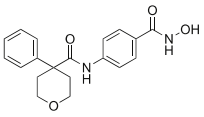	37 ± 10	28 ± 5	**34** (JT94)	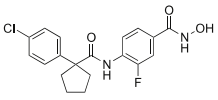	21 ± 10	774 ± 980
16		86 ± 34	12 ± 8	**35**	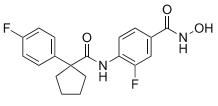	39 ± 9	204 ± 54

(*continued on next page*)

Table 1 (*continued*)

Entry	Structure	IC_{50} (nM)		Entry	Structure	IC_{50} (nM)	
		*Pf*3D7	hHDAC1			*Pf*3D7	hHDAC1
	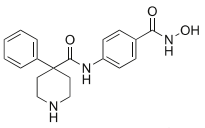						
17 (JT92)	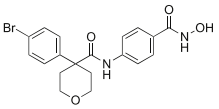	6 ± 1	2 ± 0.5	**36**	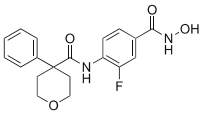	104 ± 24	73 ± 20
18	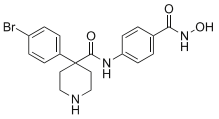	32 ± 9	3 ± 0.5	**37**	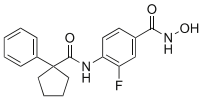	130 ± 50	181 ± 43
19 (JT21b)	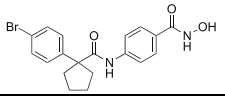	7 ± 2	7 ± 3				

interaction with the conserved Asp97 in the catalytic site of *Pf*HDAC1. This hypothesis is supported by the lower inhibitor potency when the amide bond is reversed as in **3** (IC_{50} 3.6 μM; Table 1) relative to **1** ($p = 0.0104$), this arrangement removing the putative hydrogen bond. The isopropyl group is an important component for inhibitor potency, since the phenylacetamide analogue **4** (IC_{50} 314 nM; Table 1) was 16-fold less effective than **1** ($p = 0.0003$). A phenyl ring was less preferred than the isopropyl group, since benzhydryl compound **5** (IC_{50} 140 nM; Table 1) was 7-fold less active than **1** ($p = 0.0456$). The 2-propylpentanamide **6** (IC_{50} 719 nM; Table 1) led to 36-fold less inhibition of parasite growth than for **1**, however this was not statistically significant ($p = 0.104$). The phenyl terminus may be needed for a specific protein-ligand interaction, or the flexible carbon chain was entropically disfavoured. A chlorine atom at the *ortho*-position was not well tolerated, with a 55-fold decrease in activity for **7** (IC_{50} 1.1 μM; $p < 0.0001$; Table 1). A chlorine substituent at the *meta*-position was not tolerated (**8**, $IC_{50} > 10$ μM; Table 1). An isosteric pyridine (**9**, IC_{50} 230 nM; Table 1) showed a 12-fold reduction in inhibition compared to **1** ($p = 0.001$).

The simple dimethyl analogue **10** (IC_{50} 212 nM; Table 1) was ~10-fold less effective than **1** in killing *P. falciparum* ($p < 0.0001$). Introducing a cyclopropane ring at the benzylic position (**11**) was even more disadvantageous (IC_{50} 769 nM; $p = 0.0012$; Table 1). Both the dimethyl and cyclopropane may be too small to provide an effective hydrophobic shield (Tng et al., 2020) over the amide NH···OC to maximize protein-ligand interaction. The larger but more flexible diethyl derivative **12** (IC_{50} 74 nM; Table 1) was 3–10 times more potent than **10** ($p = 0.0002$) and **11** ($p = 0.0017$). The cyclopentane ring in **13** (IC_{50} 35 nM; Table 1) conferred 2-fold higher potency than the diethyl group of **12** ($p = 0.0031$), supporting the hypothesis that a larger ring could efficiently shield the ligand-protein amide NH···OC Asp97 hydrogen bond, which would otherwise be exposed to water at the enzyme surface (Tng et al., 2020). This was further supported by cyclohexane-containing compound **14** (IC_{50} 14 nM; Table 1) inhibiting *in vitro* growth of *P. falciparum* parasites 3-fold more strongly than **13** ($p = 0.0256$). These rings also introduce some conformational rigidity. Similar to recombinant hHDAC1 enzyme inhibitory activity (Tng et al., 2020), the greater antiplasmodial activity of **14** might be attributed to a preferred conformation that placed the phenyl ring at the equatorial position and the amide axial in the cyclohexane chair conformation.

Unlike observations for inhibition of recombinant hHDAC1 (Tng et al., 2020), incorporating a polar atom at the 4-position of the cyclohexane ring to aid solvation decreased activity against *P. falciparum*. Despite double-digit nM antiplasmodial activity, the tetrahydropyran **15** (IC_{50} 37 nM; Table 1) and piperidine **16** (IC_{50} 86 nM; Table 1) were 3-fold and 6-fold less effective than **14** (IC_{50} 14 nM; $p = 0.0112$ and $p = 0.0209$, respectively; Table 1) in attenuating *P. falciparum* growth *in vitro*. One factor might be that **15** and **16** were not sufficiently hydrophobic (cLog *P* 2.2 and 2.0 respectively; ChemDraw Pro v19) for membrane permeability compared to more hydrophobic **14** (cLog *P* 3.9). Introducing a bromine atom at the *para*-position of the phenyl terminus increased cLog *P* to 3.0 and 2.8 for **17** (IC_{50} 6 nM; Table 1) and **18** (IC_{50} 32 nM; Table 1), respectively. Compounds **17** and **18** were more potent antiplasmodial inhibitors by 6- and 3-fold over **15** and **16**. Similarly, in the cyclopentane series Br-, Cl- and F-substituted derivatives **19–21** (cLog *P* 3.6–4.3) were 3–7 times more potent than unsubstituted parent compound **13** (cLog *P* 3.5) in inhibiting parasite proliferation. The halogens may block the most metabolically active position, making compounds **17–21** more stable to metabolism in *Plasmodium*-infected erythrocytes (Müller, 2004). The more hydrophobic 3-fluoro-4-trifluoromethyl analogue **22** (cLog *P* 4.6) only had modest activity (IC_{50} 233 nM). The 2-naphthalene tetrahydropyran derivative **23** (IC_{50} 32 nM, cLog *P* 3.2) was equipotent with **15**. The second benzene ring increased cLog *P* but a naphthyl group, known to be readily metabolized by CYP450 enzymes in *Plasmodium* parasites (Ndifor et al., 1990), caused **23** to be 4-fold less active than **17** ($p = 0.0151$). Replacing tetrahydropyran in **23** with cyclopentane in **24** increased cLog *P* to 4.5, reducing antiplasmodial activity 18-fold (IC_{50} 591 nM; $p = 0.0123$). A plot of *Pf*3D7 IC_{50} versus cLog *P* for representative compounds (Fig. 1) showed that, excluding **22** and **24**, there was a significant correlation of a higher IC_{50} with lower cLog *P* values (Pearson correlation coefficient, $r = -0.7787$, $p = 0.0005$). This is consistent with the need to become sufficiently hydrophobic (cLog *P* 2.8–4.3) and membrane permeable to inhibit the growth of malaria parasites.

The antiplasmodial activity of these compounds might be influenced by other parameters, such as reduced ligand complementarity at the binding pocket and reduced metabolic stability. For example, compounds **25–27** only moderately inhibited *Pf*3D7 proliferation (IC_{50} 202–441 nM; Table 1). These compounds have a metabolically unstable dimethylamine (Floyd et al., 1992), methylenedioxy moiety (Bertelsen et al., 2003) or methoxy group (Kuperman et al., 2001) on the phenyl terminus. Analogue **28** (IC_{50} 26 nM; Table 1) has a pyrazine NH that might hydrogen bond to a key residue Gly27 near the protein surface (Tng et al., 2020). If occupying the same space, the acetamido NH of **29** (IC_{50} 409 nM; Table 1) might also hydrogen bond to Gly27 and account for **30** (IC_{50} 730 nM; Table 1) being 2-fold less potent, but this does not explain why **31** (IC_{50} 683 nM; Table 1) was less potent than **29**. The imidazole scaffold **32** (IC_{50} 19 nM; Table 1) was almost equipotent with **28**. Compound **33** (IC_{50} 232 nM; Table 1) with thiazole instead of

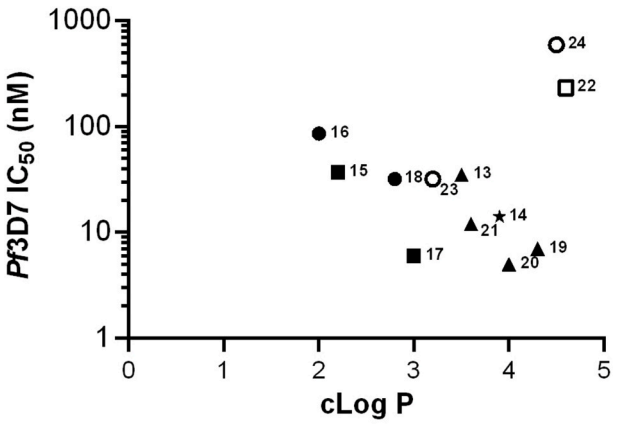

Fig. 1. Plot of *P. falciparum* 3D7 (*Pf*3D7) IC_{50} (Log10 scale) versus calculated cLog *P* for selected compounds. The compounds are grouped based on chemical structure; cyclopentane compounds **13** and **19–21** (black triangles); *N*-hydroxy-4-(1-phenylcyclohexane-1-carboxamido)benzamide **14** (black star); tetrahydropyran derivatives **15** and **17** (black squares), piperidine analogues **16** and **18** (black circles); 4-(1-(3-fluoro-4-(trifluoromethyl)phenyl)cyclopentane-1-carboxamido)-*N*-hydroxybenzamide **22** (open square); and naphthalene compounds **23** and **24** (open circles).

imidazole in **32** was 10-fold less active. The imidazole NH might be important for conferring antiplasmodial activity in addition to facilitating solubility. SAR studies of compounds **34–37** (IC_{50} 21–130 nM; Table 1) did not support an electron-withdrawing fluorine at the 3-position neighbouring the hydroxamate increasing acidity of the amide to make it a better H-bond donor. All four compounds were less effective than their parent compounds **13**, **15**, **20** and **21** in killing malaria parasites.

3.2. *P. falciparum HDAC1 homology model and ligand docking*

As there are no crystal structures of a *P. falciparum* HDAC, a Prime knowledge-based homology model of *Pf*HDAC1 (Fig. 2) was constructed using the Maestro interface to Schrodinger Suite 2020-3 (Maestro, 2020). The model had 97% Ramachandran favoured residues, a Molprobity Score (Chen et al., 2010) of 2.99, and an overall QMEAN Z-score (Benkert et al., 2011) quality estimate of −0.65. The global fold of *Pf*HDAC1 structure is characterized by a canonical arginase fold consisting of a single α/β domain, including eight β-sheets sandwiched between up to eight α-helices. Flexible loops connect the core α/β domain and smaller non-core structural elements and help form parts of the ligand binding surface (Fig. 2A). An important difference between hHDAC1 (Tng et al., 2020) and *Pf*HDAC1 near the entrance to the ligand-binding site was the insertion of residues Ala95 and Thr96 preceding Asp97 (Fig. 2B). This insert makes the corresponding *Pf*HDAC1 loop longer and potentially more flexible than in hHDAC1 and may contribute to the selectivity of some compounds in killing *P. falciparum* versus human cells (Section 3.4; Table 2). However, differences in cell permeability between infected erythrocytes and NFF cells may also play a role. We docked two of the potent compounds from Table 1, namely **19** (IC_{50} 7 nM) and **20** (IC_{50} 5 nM), into the *Pf*HDAC1 model (Fig. 3). Both compounds show hydroxamate chelated to Zn^{2+}, and three hydroxamate contacts with *Pf*HDAC1 residues namely CO···HO-Tyr301, NH···N-His139 and a water mediated hydrogen bond O···HOH···His138. In addition, the ligand aromatic ring adjacent to the hydroxamate makes π-interactions with Phe148 and Phe203. The *para*-amide substituent on

Table 2
In vitro human NFF cytotoxicity and selectivity indices versus *P. falciparum* for rac-AR-42 and analogues.

Entry	IC_{50} (nM)		Selectivity Index[a]
	*Pf*3D7	NFF	
1 (*rac*-AR-42)	22 ± 3	775 ± 169	35
4	314 ± 37	14,932 ± 1281	48
5	140 ± 64	9478 ± 3278	68
6	719 ± 583	20,180 ± 3373	28
9	230 ± 37	11,328 ± 5601	49
15	37 ± 10	809 ± 360	22
17	6 ± 1	334 ± 170	56
19	7 ± 2	532 ± 342	76
20	5 ± 3	501 ± 120	100
23	32 ± 11	165 ± 121	5
27	441 ± 46	620 ± 231	1
30	730 ± 155	209 ± 80	0.3
33	232 ± 28	433 ± 37	2
34	21 ± 10	2483 ± 1242	118

[a] Human NFF cell IC_{50}/*P. falciparum* 3D7 IC_{50}.

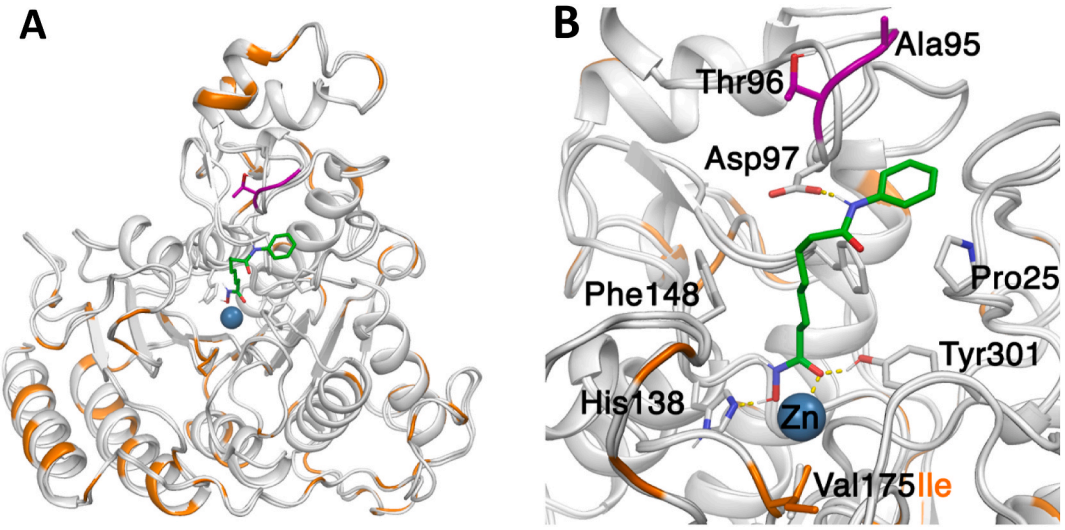

Fig. 2. (A) Homology model of *Pf*HDAC1 overlayed with the human HDAC1 (5ICN.pdb) crystal structure. The backbones of the two structures are shown, with identical residues coloured grey and non-identical hHDAC1 residues in orange. (**B**) *Pf*HDAC1 homology model showing binding site for the inhibitor SAHA (green sticks). *Pf*HDAC1 residues within 6 Å of the ligand SAHA are almost identical with hHDAC1, except for *Pf*HDAC1 Val175 which is Ile in hHDAC1 (orange sticks and label), neither of these residues contact the ligand or the binding site surface. (For interpretation of the references to colour in this figure legend, the reader is referred to the Web version of this article.)

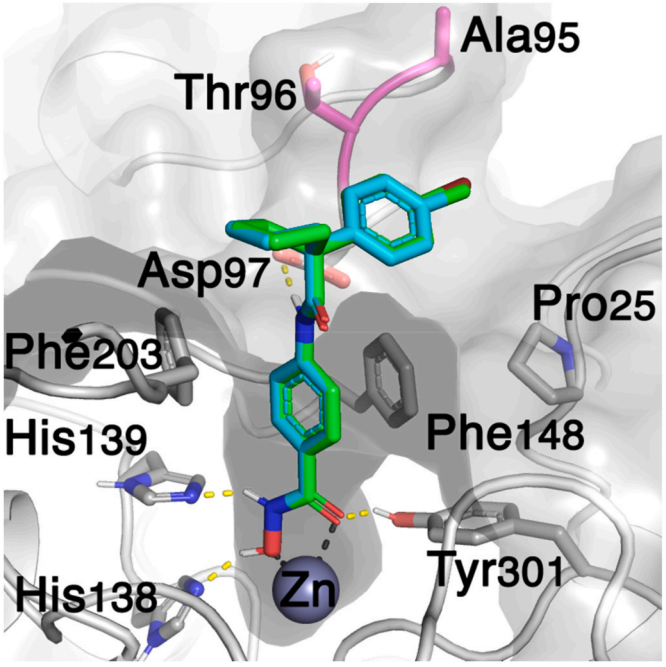

Fig. 3. *Pf*HDAC1 with Gold docked ligands 19 (JT21b, green) and 20 (JT83, cyan). *Pf*HDAC1 is shown in grey. Binding site residues are shown as sticks (carbon – grey, oxygen – red, nitrogen – blue). Ala95 and Thr96 are highlighted in magenta. H-bonds to nearby residues are shown as yellow dotted lines and interactions with Zn atom are shown as grey dotted lines. (For interpretation of the references to colour in this figure legend, the reader is referred to the Web version of this article.)

this ring makes an NH···O-Asp hydrogen bond. The cyclopentenyl group creates a hinge in the ligand to project its terminal aromatic group back towards the enzyme surface. All compounds in Table 1 are predicted to bond in a similar way to *Pf*HDAC1.

3.3. Relationship between antiplasmodial activity and human HDAC-1 inhibition

A linear correlation was discovered (Fig. 4) between inhibition of recombinant hHDAC1 and inhibition of *P. falciparum* 3D7 *in vitro* activity (Pearson correlation coefficient, r = 0.55, $\rho = 0.0005$). This suggests that the same features required to enhance hHDAC1 inhibitor potency are likely used to improve antiplasmodial activity. This finding is consistent with the high sequence and structural homology previously reported for the inhibitor-binding sites of *Pf*HDAC1 and hHDAC1 (82% similarity in catalytic domain) (Melesina et al., 2015), although we cannot conclude that these compounds only inhibit *Pf*HDAC1 among the three essential class I/II *Pf*HDAC proteins (class I *Pf*HDAC1; class II *Pf*HDA1 and *Pf*HDA2) (Andrews et al., 2012b; Kanyal et al., 2018). Recombinant *Pf*HDAC enzymes are not currently available (*Pf*HDAC1 is commercially available but has low purity (Ontoria et al., 2016)) to accurately investigate any direct inhibitory correlation between hHDAC1 and *Pf*HDACs.

Among outliers in this correlation was **34** (open square, Fig. 4), which killed malaria parasites (IC_{50} 21 nM) more effectively than inhibiting hHDAC1 (IC_{50} 774 nM). On the other hand, **23** and **29** (open triangle, Fig. 4), which were amongst the most potent inhibitors of hHDAC1, had 45-435-fold reduced antiplasmodial activity. These differences between parasite killing and hHDAC1 enzyme inhibition, despite the high chemical similarity of structures in this series, suggest that either PfHDAC1 has subtly different inhibitor binding requirements compared to hHDAC1 or, more likely, that the antiplasmodial effects of these outliers may not be exclusively through *Pf*HDAC1 inhibition.

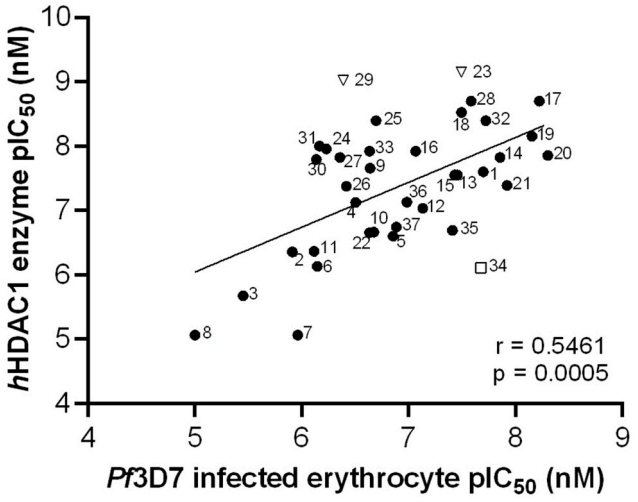

Fig. 4. Plot of recombinant human HDAC1 pIC_{50} versus *P. falciparum* 3D7 (*Pf*3D7) pIC_{50} shows that potent human HDAC1 inhibitors were often effective antiplasmodial agents *in vitro*. Pearson correlation coefficient, r = 0.5461 and $\rho = 0.0005$. Outliers include compound **34** (square), that killed malaria parasites effectively (*Pf*3D7 IC_{50} 21 nM; Table 1) but had modest inhibitory activity against hHDAC1 (IC_{50} 774 nM; Table 1) and compounds **23** and **29** (triangles) that were the most potent inhibitors of hHDAC1 (IC_{50} 0.7 nM and 0.9 nM, respectively; Table 1).

3.4. Parasite-specific selectivity of rac-AR-42 and its achiral analogues

Rac-AR-42 (**1**) and 13 other compounds were evaluated for antiproliferative activity against human neonatal foreskin fibroblasts (NFFs), as a marker of cytotoxicity (Table 2). *Rac*-AR-42 displayed 35-fold higher selectivity for killing *P. falciparum* (IC_{50} 22 nM) *versus* NFF (IC_{50} 775 nM). Achiral analogues **23**, **27**, **30** and **33** had little or no parasite-specific selectivity (SI $\leq$ 5; Table 2). Compounds **6** and **15** had more parasite-specific selectivity (SI: 22 and 28, respectively), but this was lower than that for *rac*-AR-42. Compounds **4**, **5**, 9, **17**, **19–20** and **34** demonstrated a higher selectivity index (SI: 48–118; Table 2) than *rac*-AR-42, however this level of *in vitro* selectivity would need to be improved if this chemotype were further developed for malaria.

3.5. In vivo efficacy of AR-42 and analogues in a murine model of malaria

Rac-AR-42 and four analogues **17**, **19**, **20** and **34** (designated JT92, JT21b, JT83 and JT94, respectively, for reference in future reports) were assessed for antiplasmodial activity *in vivo* in a primary screening strategy using pairs of BALB/c mice infected with *P. berghei* parasitized erythrocytes (Fig. 5). Mice were dosed orally at 25 mg/kg twice daily for four days. However, the final dose (day 3 p.i.) of **17** (both mice), **19** (both mice; Fig. 5B) or **20** (JT83; one mouse; Fig. 5D) was not given as ~10% weight loss was observed compared to day 0 (Supplementary data, Figure S3). As no additional weight loss was recorded on day 4 p.i. for mice treated with **19** or **20**, these mice continued to be monitored (Supplementary data, Figure S3; Fig. 5B and D). However, both mice in the group treated with **17** were euthanized on day 4 p.i. due to ~15% weight loss compared to day 0 (Supplementary data, Figure S3), as per approved ethics requirements. Despite the reduced dosing, no parasites were observed in the peripheral blood of mice treated with **19** or **20** up until day 24 p.i. when the experiment was ceased (Fig. 5B and D). One of two mice in the *rac*-AR-42 group developed a parasitemia on day 12 p.i., however no parasites were observed in peripheral blood smears of the second mouse (Fig. 5A). Compound **34** was the least effective, with a delayed onset of parasitemia compared to mice in the control group and no cures (Fig. 5C). While the *in vitro* antiplasmodial potency of all five

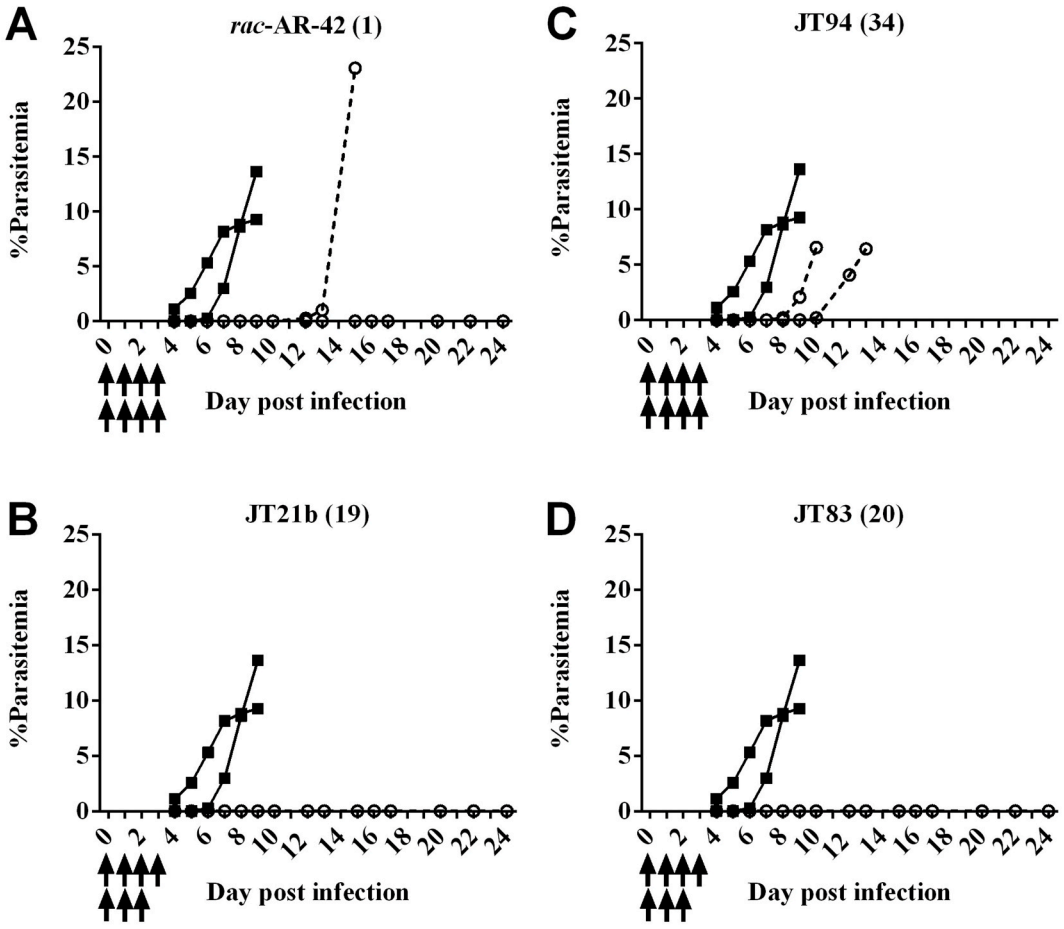

Fig. 5. ***In vivo*** **activity of orally administered AR-42 and analogues in** ***P. berghei*** **infected mice**. *P. berghei* infected BALB/c mice (two mice/group) were treated orally with 25 mg/kg AR-42 (**1**), JT21b (**19**), JT94 (**34**), JT83 (**20**) (open circles; dashed lines; **A-D**, respectively), or vehicle only (black squares; solid lines), twice daily (black arrows) for four days beginning 2 h post infection. Mice treated with **19** and **20** were not administered the final dose due to weight loss. Mean % parasitemia for individual mice is shown.

compounds was similar (*Pf*3D7 IC_{50} 5–22 nM; Table 1), unlike *rac*-AR-42 and the other analogues, **34** was the only compound with a fluorine atom on the benzene ring next to the hydroxamate zinc-binding motif, which may account for decreased *in vivo* activity.

Based on these results and the known *in vivo* pharmacokinetics and safety profile (Cheng et al., 2016; Sborov et al., 2017; Valencia et al., 2016), further *in vivo* studies were conducted on **1** as a model compound representative of this chemotype. In an initial experiment (Fig. 6A–C), groups of six mice were given **1** at 25 mg/kg once daily (q.d.; Fig. 6B) or twice daily (b.i.d.; Fig. 6C) for four consecutive days, beginning 2 h post infection (p.i.). While parasitemia was significantly attenuated from day 4–9 p.i. in the group receiving **1** q.d. compared to the vehicle control group ($p < 0.01$; Fig. 6B), mice were not cured. This result was like the HDAC inhibitor vorinostat at 25 mg/kg b.i.d. which was included as a control in this experiment (Fig. 6A). In contrast, **1** administered b.i.d. resulted in two mice developing a delayed parasitemia and required euthanasia on day 18 p.i. (Fig. 6C). The four remaining mice did not develop parasitemia for up 42 days p.i. and were considered cured (Fig. 6C). In a second experiment (Fig. 6D–F), groups of mice received oral **1** at 50 mg/kg q.d. or 25 mg/kg b.i.d. No mice developed peripheral parasitemia for up to 42 days p.i. and were considered cured (Fig. 6E and F). The difference between experiments for twice daily dosing with 25 mg/kg **1** (Fig. 6C and F) is likely due to incomplete parasite killing at this dose in all mice. In each experiment, mice in vehicle control groups all developed peripheral blood parasitemia from ~day 4 p.i. and were euthanized from day 9–10 p.i. when parasitemia reached ~20–30%, as per ethics requirements (Fig. 6).

This is the first report of any HDAC inhibitor curing *Plasmodium* infections in mice when administered orally as a monotherapy. Six HDAC inhibitors have previously been assessed for oral activity in *Plasmodium*-infected mice (Agbor-Enoh et al., 2009; Chua et al., 2017; Darkin-Rattray et al., 1996; Potluri et al., 2020; Sumanadasa et al., 2012) and, while some delayed onset of parasitemia and/or attenuated infection, none resulted in cures as a monotherapy. We speculate that superior pharmacokinetic properties of AR-42 contribute to its *in vivo* efficacy described herein. In addition to having a half-life greater than 10 h in mice following a 50 mg/kg oral single dose, the C_{max} of AR-42 at this dose (14.7 μM; Supplementary data, Table S2) (Cheng et al., 2016) is > 350-fold times higher than its potency against *P. berghei ex vivo*, determined in this study (IC_{50} 0.04 μM; Supplementary data, Figure S4). This indicates that mice are likely exposed to high enough concentrations of **1** for long enough to exert antiplasmodial activity *in vivo*. Our data also indicate that **1** has potent activity against *P. berghei* exo-erythrocytic liver stage parasites (IC_{50} 1.17 nM; Supplementary data, Figure S5), with this dual-stage activity being of interest for further investigation.

3.6. *Effect of rac-AR-42 on histone acetylation in P. falciparum*

Rac-AR-42 (**1**) was assessed for effects on *P. falciparum* histone H4 acetylation by Western blot using anti-(tetra)acetyl-H4 antibody. Compound **1**, and a reference compound vorinostat, increased *P. falciparum* histone H4 acetylation by > 2-fold compared to the vehicle control (Fig. 7). This effect was quantified using densitometry using the single ~11 kDa band corresponding to the expected size of histone H4 (Fig. 7B,

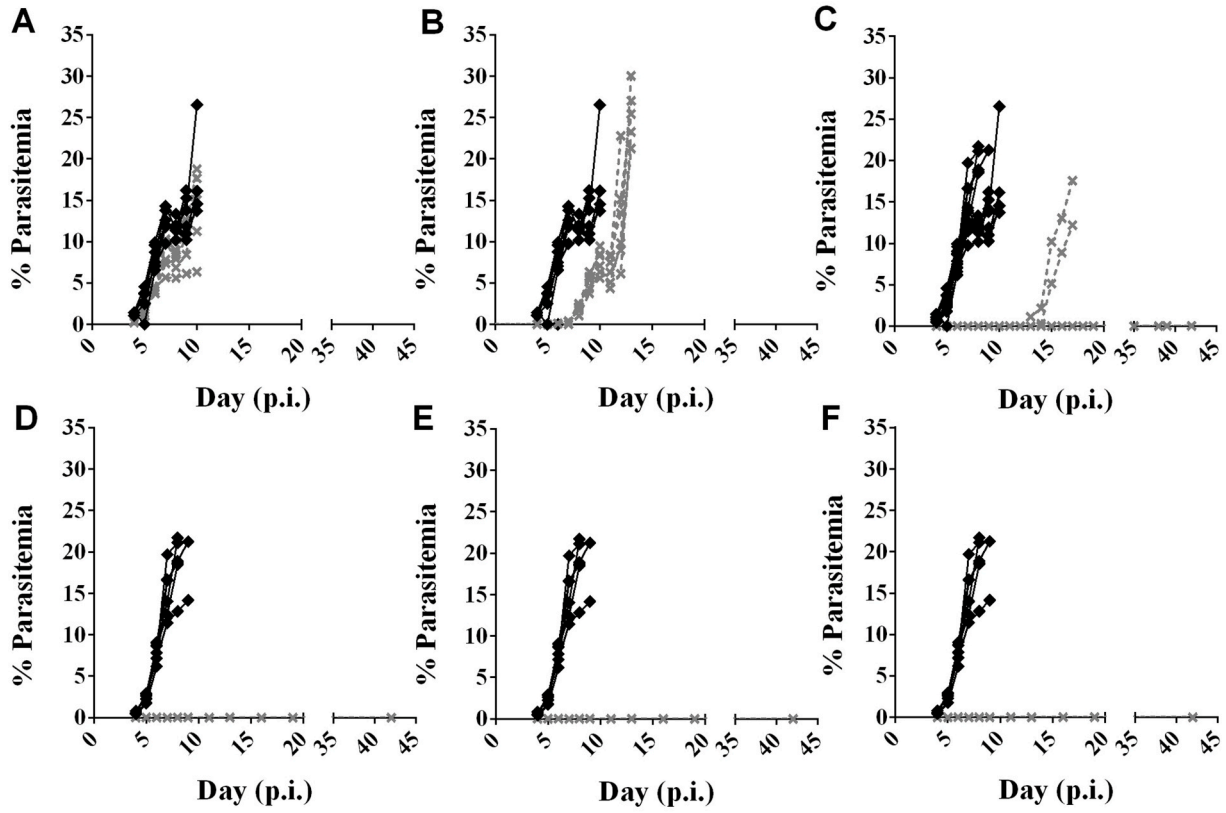

Fig. 6. *In vivo* activity of orally administered AR-42 (1) in *P. berghei* infected mice. In one experiment (**A-C**), *P. berghei* infected BALB/c mice (six mice/group) were treated orally with 25 mg/kg vorinostat (**A**; as a control) or 25 mg/kg *rac*-AR-42 (**1**) once daily (**B**) or twice daily (**C**) for four days. In a second experiment (**D-F**), *P. berghei* infected mice were treated for four days with 10 mg/kg chloroquine once daily (**D**; as a control) or 50 mg/kg **1** once daily (**E**) or 25 mg/kg **1** twice daily (**F**). Treated mice are shown with cross symbol and dashed grey lines. In each case, control mice (**A-F**; diamonds, black line) received vehicle only. Mean % parasitemia for individual mice is shown.

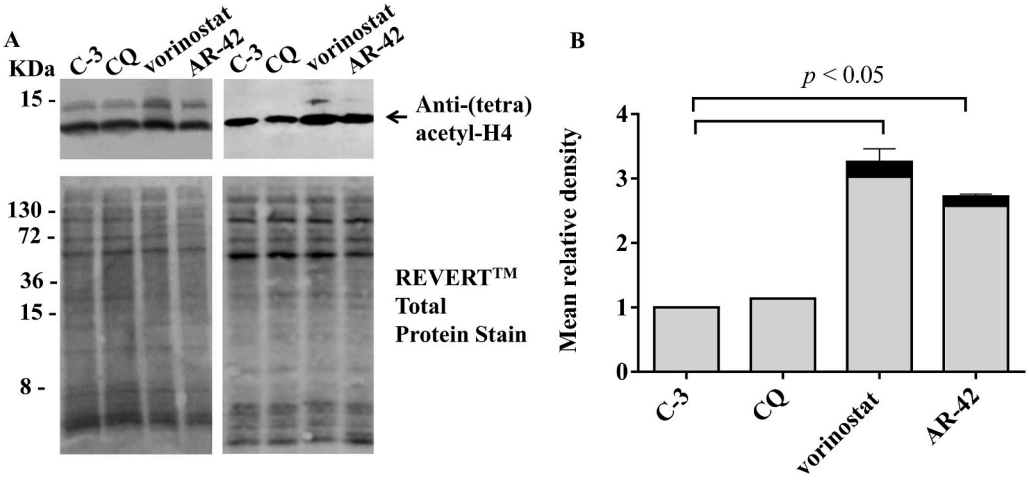

Fig. 7. Hyperacetylation of *P. falciparum* histone H4. Protein lysates were prepared from synchronous trophozoite-stage *P. falciparum* 3D7 parasites treated for 3 h with vehicle control (**C-3**; 0.1% DMSO), 5x IC_{50} compound **1**, 5x IC_{50} chloroquine (**CQ**; negative control) or 5x IC_{50} vorinostat (HDAC inhibitor control), followed by Western blot analysis. (**A**) Top panels show membrane probed with anti-(tetra)acetyl-H4 primary antibody (1:2000 dilution) and anti-rabbit IRDye® 680RD secondary antibody (1:10,000 dilution) and imaged using Odyssey® Fc Imaging System (Li-Cor Biosciences). Bottom panels show the same membranes stained with REVERT™ Total Protein Stain prior to Western blot. (**B**) Bar graph showing mean density (±SD) relative to the **C-3** DMSO control (set to 1.0) of two independent assays. Signal corresponding to H4 (~11 kDa) is shown in grey bars and total signal which includes H4 and cross-reactive bands corresponding to H2B/H2Bv (~13–14 kDa) and H2A.Z (~16 kDa) is shown in black bars.

grey), or all detectable signals (Fig. 7B; black). The higher molecular weight bands (~13–14 kDa and ~16 kDa) have been previously reported as cross-reactivity of antibody to hyperacetylated forms of H2B/H2Bv and H2A.Z, respectively (Chua et al., 2017; Engel et al., 2015; Miao et al., 2006; Sumanadasa et al., 2012). These data are consistent with **1** causing hyperacetylation of *P. falciparum* histone H4 and HDAC inhibition in *Plasmodium* parasites. Whether *Pf*HDAC1 and/or other *P. falciparum* HDACs are the targets of AR-42 remains to be determined given that pure recombinant *P. falciparum* HDACs or other molecular tools (Engel et al., 2015) to ascertain this are not available.

4. Conclusions

This study shows that inhibitors of human HDAC1 with antiplasmodial activity *in vitro* can have antimalarial activity *in vivo*. While we found that AR-42 and two achiral analogues cured *P. berghei* infections in mice, additional investigations would need to address the modest *in vitro* selectivity indices obtained for these compounds. We speculate that the improved mouse pharmacokinetic profile of AR-42 compared with clinically established HDAC inhibitors vorinostat and panobinostat (Supplementary data, Table S2) contributes to the improved activity of these compounds *in vivo*, providing proof of concept that HDAC inhibitors with a suitable pharmacodynamic and pharmacokinetic profile may be identified as new drug leads for malaria.

Declaration of competing interest

None.

Acknowledgements

We thank the Australian Red Cross Blood Service for providing human blood and sera for culture of *Plasmodium* parasites and the Griffith University Animal Facility staff.

Appendix A. Supplementary data

Supplementary data to this article can be found online at https://doi.org/10.1016/j.ijpddr.2021.08.006.

Funding

This research was supported by the National Health and Medical Research Council of Australia (NHMRC Development Grant 1093378 to KTA and DPF; Senior Principal Research Fellowship 1117017 to DPF). JT, AJL, DD, RCR and DPF thank the Australian Research Council Centre of Excellence for Advanced Molecular Imaging (grants CE140100011, DP180103244) for NMR, fluorescence and cell imaging support. MJC and EH thank Griffith University for providing academic scholarships (GUIPRS and GUPRS).

Transparency declarations

None to declare.

Author contributions

MJC, EH, GF, RCR, CDG, TS-A and KTA conducted antiplasmodial screening and mouse studies. JT, DD, RCR and DPF designed, synthesized and characterised all compounds. JT, RCR, AJC and DPF conducted modelling and analysis of structure-activity relationships. MJC, JT, RCR, DPF and KTA conceived and designed the project. All authors contributed to data analysis/interpretation, writing and editing sections of the manuscript.

References

Agbor-Enoh, S., Seudieu, C., Davidson, E., Dritschilo, A., Jung, M., 2009. Novel inhibitor of *Plasmodium* histone deacetylase that cures *P. berghei*-infected mice. Antimicrob. Agents Chemother. 53, 1727–1734.

Andrews, K.T., Fisher, G., Skinner-Adams, T.S., 2014. Drug repurposing and human parasitic protozoan diseases. Int. J. Parasitol.: Drugs Drug Resist 4, 95–111.

Andrews, K.T., Gupta, A.P., Tran, T.N., Fairlie, D.P., Gobert, G.N., Bozdech, Z., 2012a. Comparative gene expression profiling of *P. falciparum* malaria parasites exposed to three different histone deacetylase inhibitors. PloS One 7, e31847.

Andrews, K.T., Tran, T.N., Fairlie, D.P., 2012b. Towards histone deacetylase inhibitors as new antimalarial drugs. Curr. Pharmaceut. Des. 18, 3467–3479.

Andrews, K.T., Tran, T.N., Wheatley, N.C., Fairlie, D.P., 2009. Targeting histone deacetylase inhibitors for anti-malarial therapy. Curr. Top. Med. Chem. 9, 292–308.

Andrews, K.T., Walduck, A., Kelso, M.J., Fairlie, D.P., Saul, A., Parsons, P.G., 2000. Antimalarial effect of histone deacetylation inhibitors and mammalian tumour cytodifferentiating agents. Int. J. Parasitol. 30, 761–768.

Bechtsi, D.P., Waters, A.P., 2017. Genomics and epigenetics of sexual commitment in *Plasmodium*. Int. J. Parasitol. 47, 425–434.

Benkert, P., Biasini, M., Schwede, T., 2011. Toward the estimation of the absolute quality of individual protein structure models. Bioinformatics 27, 343–350.

Bertelsen, K.M., Venkatakrishnan, K., Von Moltke, L.L., Obach, R.S., Greenblatt, D.J., 2003. Apparent mechanism-based inhibition of human CYP2D6 in vitro by paroxetine: comparison with fluoxetine and quinidine. Drug Metab. Dispos. 31, 289–293.

Bozdech, Z., Llinas, M., Pulliam, B.L., Wong, E.D., Zhu, J., DeRisi, J.L., 2003. The transcriptome of the intraerythrocytic developmental cycle of *Plasmodium falciparum*. PLoS Biol. 1, E5.

Burrows, J.N., Duparc, S., Gutteridge, W.E., Hooft van Huijsduijnen, R., Kaszubska, W., Macintyre, F., Mazzuri, S., Mohrle, J.J., Wells, T.N.C., 2017. New developments in anti-malarial target candidate and product profiles. Malar. J. 16, 26.

Chaal, B.K., Gupta, A.P., Wastuwidyaningtyas, B.D., Luah, Y.-H., Bozdech, Z., 2010. Histone deacetylases play a major role in the transcriptional regulation of the *Plasmodium falciparum* life cycle. PLoS Pathog. 6, e1000737.

Chen, V.B., Arendall 3rd, W.B., Headd, J.J., Keedy, D.A., Immormino, R.M., Kapral, G.J., Murray, L.W., Richardson, J.S., Richardson, D.C., 2010. MolProbity: all-atom structure validation for macromolecular crystallography. Acta Crystallogr. D Biol. Crystallogr. 66, 12–21.

Chen, Y.-J., Wang, W.-H., Wu, W.-Y., Hsu, C.-C., Wei, L.-R., Wang, S.-F., Hsu, Y.-W., Liaw, C.-C., Tsai, W.-C., 2017. Novel histone deacetylase inhibitor AR-42 exhibits antitumor activity in pancreatic cancer cells by affecting multiple biochemical pathways. PloS One 12, e0183368.

Cheng, H., Xie, Z., Jones, W.P., Wei, X.T., Liu, Z., Wang, D., Kulp, S.K., Wang, J., Coss, C. C., Chen, C.-S., Marcucci, G., Garzon, R., Covey, J.M., Phelps, M.A., Chan, K.K., 2016. Preclinical pharmacokinetics study of R- and S-enantiomers of the histone deacetylase inhibitor, AR-42 (NSC 731438), in rodents. AAPS J. 18, 737–745.

Chua, M.J., Arnold, M.S.J., Xu, W., Lancelot, J., Lamotte, S., Späth, G.F., Prina, E., Pierce, R.J., Fairlie, D.P., Skinner-Adams, T.S., Andrews, K.T., 2017. Effect of clinically approved HDAC inhibitors on *Plasmodium, Leishmania* and *Schistosoma* parasite growth. Int. J. Parasitol.: Drugs and Drug Resistance 7, 42–50.

ClinicalTrials.gov, 2017a. AR-42 in Treating Patients with Advanced or Relapsed Multiple Myeloma, Chronic Lymphocytic Leukemia or Lymphoma.

ClinicalTrials.gov, 2017b. Exploratory Evaluation of AR-42 Histone Deacetylase Inhibitor in the Treatment of Vestibular Schwannoma and Meningioma.

Coetzee, N., von Gruning, H., Opperman, D., van der Watt, M., Reader, J., Birkholtz, L. M., 2020. Epigenetic inhibitors target multiple stages of *Plasmodium falciparum* parasites. Sci. Rep. 10, 2355.

Coleman, B.I., Skillman, K.M., Jiang, R.H.Y., Childs, L.M., Altenhofen, L.M., Ganter, M., Leung, Y., Goldowitz, I., Kafsack, B.F.C., Marti, M., Llinas, M., Buckee, C.O., Duraisingh, M.T., 2014. A *Plasmodium falciparum* histone deacetylase regulates antigenic variation and gametocyte conversion. Cell Host Microbe 16, 177–186.

Darkin-Rattray, S.J., Gurnett, A.M., Myers, R.W., Dulski, P.M., Crumley, T.M., Allocco, J. J., Cannova, C., Meinke, P.T., Colletti, S.L., Bednarek, M.A., Singh, S.B., Goetz, M.A., Dombrowski, A.W., Polishook, J.D., Schmatz, D.M., 1996. Apicidin: a novel antiprotozoal agent that inhibits parasite histone deacetylase. Proc. Natl. Acad. Sci. U.S.A. 93, 13143–13147.

Dow, G.S., Chen, Y., Andrews, K.T., Caridha, D., Gerena, L., Gettayacamin, M., Johnson, J., Li, Q., Melendez, V., Obaldia, N., Tran, T.N., Kozikowski, A.P., 2008. Antimalarial activity of phenylthiazolyl-bearing hydroxamate-based histone deacetylase inhibitors. Antimicrob. Agents Chemother. 52, 3467–3477.

Duraisingh, M.T., Voss, T.S., Marty, A.J., Duffy, M.F., Good, R.T., Thompson, J.K., Freitas-Junior, L.H., Scherf, A., Crabb, B.S., Cowman, A.F., 2005. Heterochromatin silencing and locus repositioning linked to regulation of virulence genes in *Plasmodium falciparum*. Cell 121, 13–24.

Engel, J.A., Jones, A.J., Avery, V.M., Sumanadasa, S.D.M., Ng, S.S., Fairlie, D.P., Adams, T.S., Andrews, K.T., 2015. Profiling the anti-protozoal activity of anti-cancer HDAC inhibitors against *Plasmodium* and *Trypanosoma* parasites. Int. J. Parasitol.: Drugs and Drug Resistance 5, 117–126.

Floyd, D.M., Kimball, S.D., Krapcho, J., Das, J., Turk, C.F., Moquin, R.V., Lago, M.W., Duff, K.J., Lee, V.G., White, R.E., et al., 1992. Benzazepinone calcium channel blockers. 2. Structure-activity and drug metabolism studies leading to potent antihypertensive agents. Comparison with benzothiazepinones. J. Med. Chem. 35, 756–772.

Freitas-Junior, L.H., Hernandez-Rivas, R., Ralph, S.A., Montiel-Condado, D., Ruvalcaba-Salazar, O.K., Rojas-Meza, A.P., Mancio-Silva, L., Leal-Silvestre, R.J., Gontijo, A.M., Shorte, S., Scherf, A., 2005. Telomeric heterochromatin propagation and histone acetylation control mutually exclusive expression of antigenic variation genes in malaria parasites. Cell 121, 25–36.

Huber, W., Koella, J.C., 1993. A comparison of three methods of estimating EC50 in studies of drug resistance of malaria parasites. Acta Trop. 55, 257–261.

Kanyal, A., Rawat, M., Gurung, P., Choubey, D., Anamika, K., Karmodiya, K., 2018. Genome-wide survey and phylogenetic analysis of histone acetyltransferases and histone deacetylases of *Plasmodium falciparum*. FEBS J. 285, 1767–1782.

Kuperman, A.V., Kalgutkar, A.S., Marfat, A., Chambers, R.J., Liston, T.E., 2001. Pharmacokinetics and metabolism of a cysteinyl leukotriene-1 receptor antagonist from the heterocyclic chromanol series in rats: in vitro-in vivo correlation, gender-related differences, isoform identification, and comparison with metabolism in human hepatic tissue. Drug Metab. Dispos. 29, 1403–1409.

Lopez-Rubio, J.J., Gontijo, A.M., Nunes, M.C., Issar, N., Hernandez Rivas, R., Scherf, A., 2007. 5' flanking region of var genes nucleate histone modification patterns linked

to phenotypic inheritance of virulence traits in malaria parasites. Mol. Microbiol. 66, 1296–1305.
Lu, Q., Wang, D.S., Chen, C.S., Hu, Y.D., Chen, C.S., 2005. Structure-based optimization of phenylbutyrate-derived histone deacetylase inhibitors. J. Med. Chem. 48, 5530–5535.
Lu, Q., Yang, Y.T., Chen, C.S., Davis, M., Byrd, J.C., Etherton, M.R., Umar, A., Chen, C.S., 2004. Zn2+-chelating motif-tethered short-chain fatty acids as a novel class of histone deacetylase inhibitors. J. Med. Chem. 47, 467–474.
Maestro, 2020. Schrodinger Release, vols. vols. 2020–3. Schrodinger, LLC, New York, NY.
Malmquist, N.A., Moss, T.A., Mecheri, S., Scherf, A., Fuchter, M.J., 2012. Small-molecule histone methyltransferase inhibitors display rapid antimalarial activity against all blood stage forms in *Plasmodium falciparum*. Proc. Natl. Acad. Sci. U.S.A. 109, 16708–16713.
Melesina, J., Robaa, D., Pierce, R.J., Romier, C., Sippl, W., 2015. Homology modeling of parasite histone deacetylases to guide the structure-based design of selective inhibitors. J. Mol. Graph. Model. 62, 342–361.
Miao, J., Fan, Q., Cui, L., Li, J., Li, J., Cui, L., 2006. The malaria parasite *Plasmodium falciparum* histones: Organization, expression, and acetylation. Gene 369, 53–65.
Müller, S., 2004. Redox and antioxidant systems of the malaria parasite *Plasmodium falciparum*. Mol. Microbiol. 53, 1291–1305.
Ndifor, A.M., Ward, S.A., Howells, R.E., 1990. Cytochrome P-450 activity in malarial parasites and its possible relationship to chloroquine resistance. Mol. Biochem. Parasitol. 41, 251–257.
Ontoria, J.M., Paonessa, G., Ponzi, S., Ferrigno, F., Nizi, E., Biancofiore, I., Malancona, S., Graziani, R., Roberts, D., Willis, P., Bresciani, A., Gennari, N., Cecchetti, O., Monteagudo, E., Orsale, M.V., Veneziano, M., Di Marco, A., Cellucci, A., Laufer, R., Altamura, S., Summa, V., Harper, S., 2016. Discovery of a selective series of inhibitors of *Plasmodium falciparum* HDACs. ACS Med. Chem. Lett. 7, 454–459.
Phillips, M.A., Burrows, J.N., Manyando, C., van Huijsduijnen, R.H., Van Voorhis, W.C., Wells, T.N.C., 2017. Malaria. Nat Rev Dis Primers 3, 17050.
Potluri, V., Shandil, R.K., Gavara, R., Sambasivam, G., Campo, B., Wittlin, S., Narayanan, S., 2020. Discovery of FNDR-20123, a histone deacetylase inhibitor for the treatment of *Plasmodium falciparum* malaria. Malar. J. 19, 365.
Saul, A., Prescott, N., Smith, F., Cheng, Q., Walliker, D., 1997. Evidence of cross-contamination among laboratory lines of *Plasmodium berghei*. Mol. Biochem. Parasitol. 84, 143–147.
Sborov, D.W., Canella, A., Hade, E.M., Mo, X., Khountham, S., Wang, J., Ni, W., Poi, M., Coss, C., Liu, Z., Phelps, M.A., Mortazavi, A., Andritsos, L., Baiocchi, R.A., Christian, B.A., Benson, D.M., Flynn, J., Porcu, P., Byrd, J.C., Pichiorri, F., Hofmeister, C.C., 2017. A phase 1 trial of the HDAC inhibitor AR-42 in patients with multiple myeloma and T- and B-cell lymphomas. Leuk. Lymphoma 58, 2310–2318.
Sumanadasa, S.D., Goodman, C.D., Lucke, A.J., Skinner-Adams, T., Sahama, I., Haque, A., Do, T.A., McFadden, G.I., Fairlie, D.P., Andrews, K.T., 2012. Antimalarial activity of the anticancer histone deacetylase inhibitor SB939. Antimicrob. Agents Chemother. 56, 3849–3856.
Tng, J., Lim, J., Wu, K.C., Lucke, A.J., Xu, W., Reid, R.C., Fairlie, D.P., 2020. Achiral derivatives of hydroxamate AR-42 potently inhibit class I HDAC enzymes and cancer cell proliferation. J. Med. Chem. 63, 5956–5971.
Trenholme, K., Marek, L., Duffy, S., Pradel, G., Fisher, G., Hansen, F.K., Skinner-Adams, T.S., Butterworth, A., Ngwa, C.J., Moecking, J., Goodman, C.D., McFadden, G.I., Sumanadasa, S.D.M., Fairlie, D.P., Avery, V.M., Kurz, T., Andrews, K.T., 2014. Lysine acetylation in sexual stage malaria parasites is a target for antimalarial small molecules. Antimicrob. Agents Chemother. 58, 3666–3678.
Valencia, H., Newton, H.B., Hade, E., Sborov, D.W., Cavaliere, R., Poi, M., Phelps, M., Wang, J., Coss, C.C., Khountham, S., Monk, P., Olencki, T., Shapiro, C.L., Piekarz, R., Hofmeister, C.C., Grever, M.R., Welling, D.B., Mortazavi, A., 2016. A phase 1 study of AR-42 in patients with advanced solid tumors, including nervous system tumors. J. Clin. Oncol. 34, 2558-2558.
Vanheer, L.N., Zhang, H., Lin, G., Kafsack, B.F.C., 2020. Activity of epigenetic inhibitors against *Plasmodium falciparum* asexual and sexual blood stages. Antimicrob. Agents Chemother. 64.
World Health Organization, 2020. World Malaria Report 2020.